ELSEVIER

Finite Element Analysis of Partially Prestressed Steel Fiber Concrete Beams in Shear

P. Paramasivam,* Kiang-Hwee Tan,* and K. Murugappan†
*Department of Civil Engineering, National University of Singapore and †Dr. Lee Chiaw Meng Associate, Singapore

This paper presents a finite element formulation for the modeling of the behavior of partially prestressed steel fiber concrete beams in shear. Based on a secant modulus approach, the formulation treats steel fiber concrete as an orthotropic material, characterized by appropriate constitutive relations in the principal compressive and tensile directions. An experimental program with the partial prestressing ratio, the shear span:effective depth ratio, and the volume fraction of steel fibers as test variables was carried out and the deflections of the beam, concrete, and steel strains were monitored and compared with the results of the finite element analysis. The finite element formulation was found to predict the deformational characteristics and the ultimate load of the test beams well. Steel fibers were observed to improve the beam stiffness after the occurrence of first shear crack and to enhance the shear strength of partially prestressed concrete beams significantly. ADVANCED CEMENT BASED MATERIALS 1995, 2, 231–239

KEY WORDS: Beams, Finite element analysis, Partial prestressing, Shear strength, Steel fiber concrete, Steel fibers

Many studies have been carried out on the use of steel fibers in reinforced concrete beams as shear reinforcement. There is a general consensus that the steel fibers are efficient in taking up shear, which may lead to a change of the mode of failure of beams from shear to flexure [1–6]. Recent studies on reinforced steel fiber concrete (SFC) beams [7] also suggested that, in addition to the increase in the ultimate shear capacity, there is a reduction in strains in the steel reinforcement and concrete by the addition of steel fibers.

There have been a limited number of studies that reported on the use of steel fibers in partially prestressed concrete beams. One of the earlier studies in this area was reported by Balaguru et al. [8], who investigated the ultimate shear capacity of high strength partially prestressed SFC beams. The study indicated that there was only a marginal increase in the shear strength due to the addition of steel fibers. However, steel fibers were found to control crack widths and steel strains significantly. On the other hand, experimental studies by Narayanan et al. [9] on rectangular partially prestressed SFC beams indicated that fibers contributed to a significant increase in the shear strength. Based on their observations, Narayanan et al. suggested equations for the ultimate shear strength, which are modifications of the equations given by the British Standard [10] for conventionally reinforced concrete beams.

In this study, a finite element formulation was developed to model the behavior of partially prestressed SFC beams in shear. Also, a systematic experimental study was carried out to verify the predictive capability of the analytical formulation. The test results are presented and discussed with respect to the influencing parameters.

Finite Element Formulation

In this formulation, the reinforcements were assumed to be elastic-perfectly plastic and the steel fiber concrete (SFC) was treated as an orthotropic, non-linear elastic material with stress-strain relations in two principal directions. A smeared rotating crack model with four-noded quadrilateral finite elements was used and the solution was obtained via a secant modulus approach.

Constitutive Relations for Steel Fiber Concrete

PRINCIPAL COMPRESSIVE STRESS-STRAIN RELATION. The principal compressive stress-strain relation accounting for the softening of concrete under biaxial compression-tension is expressed in terms of the uniaxial compres-

Address correspondence to: Kiang-Hwee Tan, Department of Civil Engineering, National University of Singapore, 10 Kent Ridge Crescent, Singapore 0511, Singapore.
Received July 27, 1994; Accepted March 3, 1995

ISSN 1065-7355/95/$9.50
SSDI 1065-7355(95)00020-R

sive strength of the SFC cylinders, f_c', and the corresponding axial strain, ϵ_0, as (see Figure 1a):

$$\sigma_d = f_{c2max}\left[2\left(\frac{\epsilon_d}{\epsilon_0}\right) - \left(\frac{\epsilon_d}{\epsilon_0}\right)^2\right] \tag{1}$$

$$\text{where } \frac{f_{c2max}}{f_c'} = \left(\frac{1.0}{0.8 - 0.34\frac{\epsilon_r}{\epsilon_0}}\right) \leq 1.0$$

in which ϵ_d and ϵ_r are, respectively, the principal compressive and tensile strains, and σ_d is the principal compressive stress.

PRINCIPAL TENSILE STRESS-STRAIN RELATION. The principal tensile stress-strain relation has two distinct portions, one before cracking and the other after cracking (see Figure 1b). Before cracking, the behavior is assumed to be elastic and the principal tensile stress-strain relation is given as [7]:

$$\sigma_r = \epsilon_r E_c \text{ for } \epsilon_r \leq \epsilon_{cr} \tag{2}$$

where E_c is the Young's modulus and ϵ_{cr} is the cracking strain of steel fiber concrete. The cracking strain ϵ_{cr} is computed as $\epsilon_{cr} = f_{cr}/E_c$, with f_{cr} and E_c taken as:

$$f_{cr} = 0.33\sqrt{f_c'} \text{ (MPa)} \tag{3}$$

$$E_c = 2f_c' / \epsilon_0 \tag{4}$$

The average principal tensile stress-strain relation after cracking is given by [7]:

$$\sigma_r = \frac{f_{cr} + (\beta\,\sigma_{tu})}{1 + \beta} \text{ for } \epsilon_r > \epsilon_{cr} \tag{5}$$

$$\text{where } \beta = \sqrt{\frac{\epsilon_r - \epsilon_{cr}}{0.005}}$$

The value of the postcracking tensile strength, σ_{tu}, depends on the orientation factor η_0', the length efficiency factor η_1, the volume fraction V_f, and the ultimate bond strength, τ_u, of the fibers and can be taken as [11]:

$$\sigma_{tu} = \frac{\eta_1\,\eta_0'\,V_f\,l_f\,\tau_u}{2r'} \tag{6}$$

where l_f is the length of the fibers and r' is the ratio of area to perimeter of the steel fibers.

It should be noted that the above principal tensile stress-strain relation overestimates the residual strength for the case where there is little or no reinforcement. The validity of these relations was discussed in Tan et al. [7] and Murugappan et al. [12].

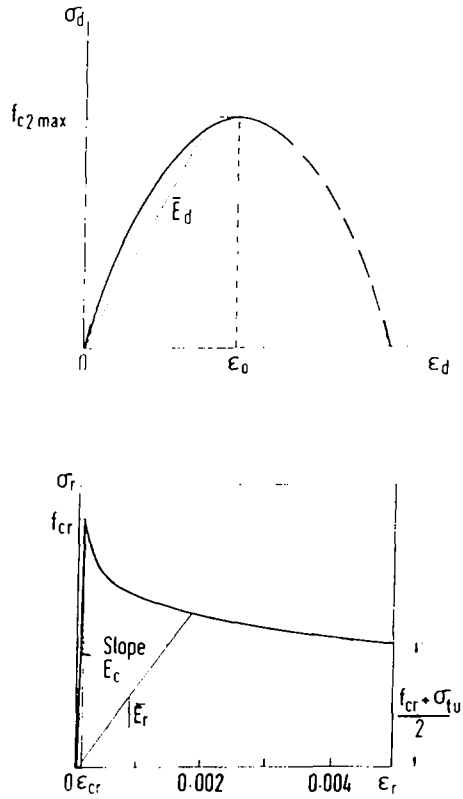

FIGURE 1. (a) Principal compressive stress-strain relation for steel fiber concrete (SFC). (b) Principal tensile stress-strain relation for SFC.

Stiffness Matrices

The state of stress in a cracked element located in the shear span of a beam is shown in Figure 2. The element is under a biaxial state of stress, with shear stresses acting along four sides. The load acting on the cracked element can be considered as a sum of the load taken up by the steel elements and the cracked SFC element. The cracked SFC is modeled as an orthotropic material with the principal compressive and tensile directions denoted by d and r respectively. Assuming that the Poisson's effect is negligible after cracking, the material stiffness for SFC in the principal directions $[D_c']$ is given by [13]:

$$[D_c'] = \begin{bmatrix} \bar{E}_d & 0 & 0 \\ 0 & \bar{E}_r & 0 \\ 0 & 0 & \bar{G} \end{bmatrix} \tag{7}$$

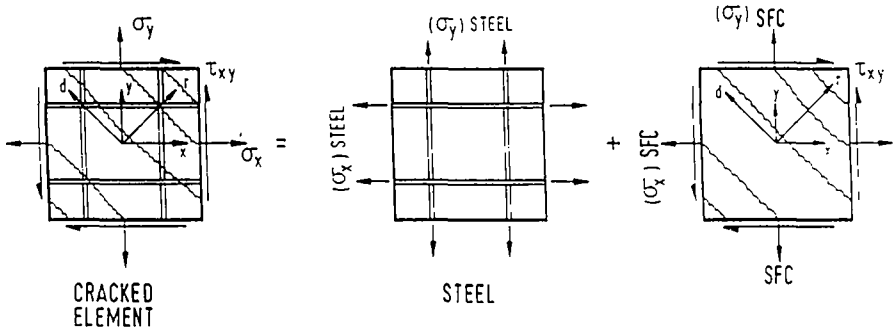

FIGURE 2. State of stress in a cracked steel fiber concrete element.

where $\bar{E}_r$ and $\bar{E}_d$ are the secant moduli in the principal tensile and compressive directions, respectively, and $\bar{G}$ is the secant shear modulus. The secant moduli $\bar{E}_r$, $\bar{E}_d$, and $\bar{G}$ are computed using the principal compressive and principal tensile stress-strain relations for SFC as given in eqs 1 to 6, that is:

$$\bar{E}_r = \frac{\sigma_r}{\epsilon_r}, \quad \bar{E}_d = \frac{\sigma_d}{\epsilon_d} \text{ and } \bar{G} = \frac{\bar{E}_r \bar{E}_d}{\bar{E}_r + \bar{E}_d} \tag{8}$$

where, σ_r and σ_d are the principal tensile stress and compressive stress, respectively, and ϵ_r and ϵ_d are the corresponding strains. It is assumed in this formulation that the average strains in SFC and steel in an element are the same, which indirectly allows for local slipping of reinforcement to occur at crack locations. The material stiffness matrix for the reinforcement component i along its axis is computed as:

$$[D'_{si}] = \begin{bmatrix} \rho_{si} \bar{E}_i & 0 & 0 \\ 0 & 0 & 0 \\ 0 & 0 & 0 \end{bmatrix} \tag{9}$$

where E_i is the secant modulus and ρ_{si} is the ratio of steel reinforcement in the ith direction. In the present study, prestressed and non-prestressed steels were modeled as elastic-perfectly plastic materials.

The material stiffness matrix for the element $[D]$ is obtained after transformation to global coordinates, as:

$$\begin{aligned} [D] &= [D_c] + [D_s] \\ [D_c] &= [T_c]^T [D'_c] [T_c] \\ [D_s] &= \sum_{i=1}^{n} [T_{si}]^T [D'_{si}] [T_{si}] \end{aligned} \tag{10}$$

where $[D'_c]$ and $[D'_{si}]$ are the material stiffness matrices for SFC and steel respectively; and $[T_c]$ and $[T_{si}]$ are the corresponding transformation matrices. Once the material stiffness matrix is obtained, the element stiffness can be computed as $\int [B]^T [D] [B] \, dV$, where $[B]$ is the strain shape function for a four-noded quadrilateral linear displacement element [12].

Governing Equations and Solution Procedure

The prestrain in the SFC and steel bars are computed by using a pseudoforce approach [13]. With

$$\{\epsilon_c^o\} = \begin{Bmatrix} \epsilon_{cx}^o \\ \epsilon_{cy}^o \\ \epsilon_{cxy}^o \end{Bmatrix} \text{ and } \{\epsilon_{si}^o\} = \begin{Bmatrix} \epsilon_{sxi}^o \\ \epsilon_{syi}^o \\ \epsilon_{sxyi}^o \end{Bmatrix} \tag{11}$$

where $\{\epsilon_c^o\}$ and $\{\epsilon_{si}^o\}$ are the prestrains in the SFC and steel bars, respectively, expressed in the global coordinates, the prestrain joint forces $\{F^*\}^e$ on an element, e, can be computed as:

$$\{F^*\}^e = \int_v [B]^T [D_c] \{\epsilon_c^o\} \, dV + \sum_{i=1}^{n} \int_v [B]^T [D_{si}] \{\epsilon_{si}^o\} \, dV \tag{12}$$

The prestrain forces are added to the externally applied joint loads $\{F\}$ to obtain the total force vector and the final equation is given as:

$$\{F\} + \{F^*\} = [K] \{\delta\} \tag{13}$$

where $[K]$ is the global stiffness matrix and $\{\delta\}$ is the nodal displacement vector. However, it should be noted that for each iteration at a load level, the pseudo force vector $\{F\}^*$is calculated based on the secant moduli corresponding to that iteration.

The finite element solution is based on the total stress-strain formulation, and a simple iterative procedure is adopted to obtain the solution. The element stiffness matrices are initialized with the elastic constants for the first iteration. For subsequent iterations, the secant moduli are computed based on the state of

strain in the element. The iterative procedure is continued till the convergence is obtained. More details on the solution procedure and the numerical stability can be found in Vecchio [13] and Murugappan et al. [12].

Experimental Program

A total of eight T beams were tested. All the beams were simply supported and subjected to a symmetrical two-point loading, typically shown in Figure 3a. All the beams had an effective depth of 185 mm. The length of the constant moment zone was 200 mm for specimen TB25 and 300 mm for all the other beams. The shear span was adjusted to obtain the required shear span:effective depth ratio. The beams had both prestressed and non-prestressed reinforcements in the tensile zone. The extent of the prestressing in the beams is quantified by the partial prestressing ratio (PPR), defined as the ratio of the ultimate resisting moment due to the prestressed reinforcement $(M_u)_p$ to the ultimate resisting moment due to all tensile steel $(M_u)_{p+s}$ [14], that is,

$$\text{PPR} = \frac{(M_u)_p}{(M_u)_{p+s}} \tag{14}$$

The centroids of the prestressed and the non-prestressed reinforcement were at the same level for all the beams in the present study. Also, the section was designed such that both the prestressed and non-prestressed steel yield, when subjected to the ultimate moment. Therefore, eq 14 can be reduced to:

$$\text{PPR} = \frac{A_{ps} f_{py}}{A_{ps} f_{py} + A_s f_y} \tag{15}$$

where A_s and A_{ps} are, respectively, the area of the non-prestressed and prestressed reinforcement, and f_y and f_{py} are the corresponding yield strengths.

All the prestressing steel was stressed to approximately 70% of their yield strength f_{py}. Sufficient development length at the ends of the beam was provided for the prestressed reinforcement to ensure proper anchorage. The details of the reinforcements for the beams with PPR of 0.0, 0.25, 0.5, and 1.0 are also shown in Figure 3b. The volume fraction of steel fibers varied from 0.0 to 1.0%. The complete details of the test program is given in Table 1.

The SFC mix was designed for a target cylinder strength of 40 MPa. The actual values of the cylinder strength for all the beams are given in Table 1. The concrete mix proportion used was 1:1.2:1.2 by weight of cement, sand, and coarse aggregate, respectively, with a water:cement ratio of 0.45. A rapid hardener was used to obtain high early strength. The cement content was kept high and the amount of coarse aggregate was kept low to ensure good workability with the addition of steel fibers. No problems were encoun-

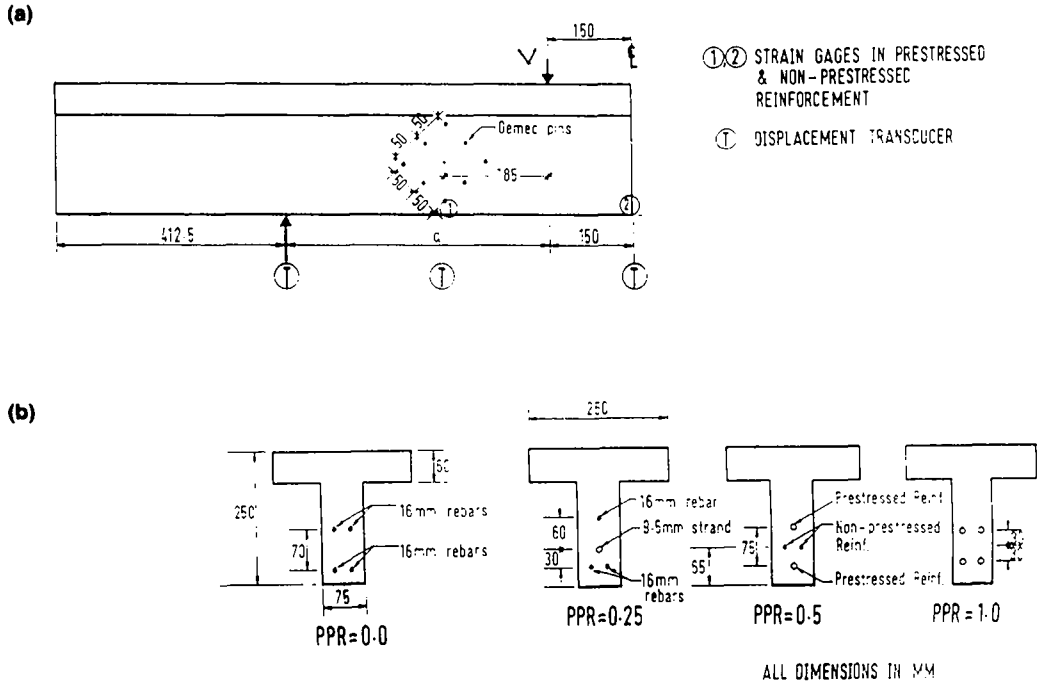

FIGURE 3. (a) Test set-up and loading arrangement. (b) Details of the beam section at A-A.

TABLE 1. Details of test beams

Designation	a:d	V_f (%)	Partial Prestressing Ratio	f'_c (MPa)
TB21	2.5	0.0	0.50	33.7
TB22	2.5	0.5	0.50	34.7
TB23	2.5	1.0	0.50	40.5
TB24	2.0	1.0	0.50	42.3
TB25	3.0	1.0	0.50	38.2
TB26	2.5	1.0	0.25	39.1
TB27	2.5	1.0	0.00	38.5
TB28	2.5	1.0	1.00	34.0

tered during mixing and placing even with 1% volume fraction of fibers.

Seven wire strands with a nominal diameter of 9.5 mm were used as prestressed reinforcement. The strand had an average yield strength f_{py} of 1,894 MPa (at 1% strain). The reinforcing bars were 16 mm in diameter and had an average yield strength of 527 MPa and a modulus of elasticity of 200 GPa.

Electrical strain gauges were fixed to the non-prestressed reinforcement at three different locations as indicated in Figure 3a. At least two strain gauges were fixed at each location. The size of the strain gauge base was 5.0 mm × 16.0 mm. Strain gauges were fixed to the single wires of the prestressed strands in the shear span and midspan as shown in Figure 3a. The base of these strain gauges was of the size 1.5 mm × 5.0 mm. Because the wires are spirally oriented to the axis of the strand, the apparent modulus obtained from tension tests with the strain gauges fixed in the same way as in the test beams was used to obtain stresses from the measured strains. The apparent modulus was found to be 220 GPa for the strands.

A 10 m long prestressing bed was used to cast the beams. The reinforcement cage was first placed in the mold with the spacers. Later, the prestressing strands were aligned and kept in position using the grips fixed on both ends of the prestressing bed. Prestressing was done with a hydraulic jack. A slightly higher pressure than that computed to achieve 0.7 f_{py} was applied on the ram, so that after the initial slip, the stress in the prestressing strand would be approximately 0.7 f_{py}. Also, the strains in the strands were monitored along with the pressure gauge readings. Before casting, strain measurements were obtained from the strain gauges fixed to the prestressing strands, and the prestressing force in the strand was computed. The beams were cast and cured by covering with wet gunny sacks. The prestressing strands were cut 3 days after casting. The beams were then white-washed and the demec pins fixed in the arrangement as shown in Figure 3a to monitor the concrete surface strains during testing. The demec gauge had a gauge length of 100 mm. To obtain the average strain in each direction, three pairs of demec pins were fixed on the shear span on each side of the beam. This ensures that "average" strains are obtained and the measurements accurately reflect the concrete deformations, including the first shear cracking load.

The test was carried out using a testing machine with displacement control, with a maximum capacity of 500 kN. The deflection of the beams was monitored at five locations. The final midspan deflections were obtained after accounting for any support settlement. The location of the displacement transducers is also shown in Figure 3a. The data from the strain gauges and the displacement transducers was acquired using a data logging system and recorded for every 5 kN load

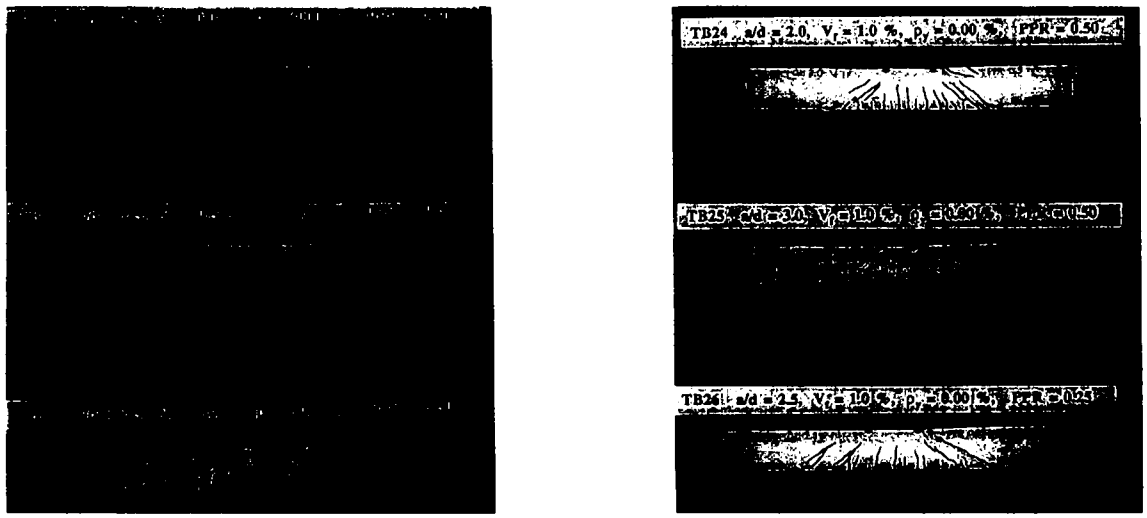

FIGURE 4. Typical failure patterns of the beams tested.

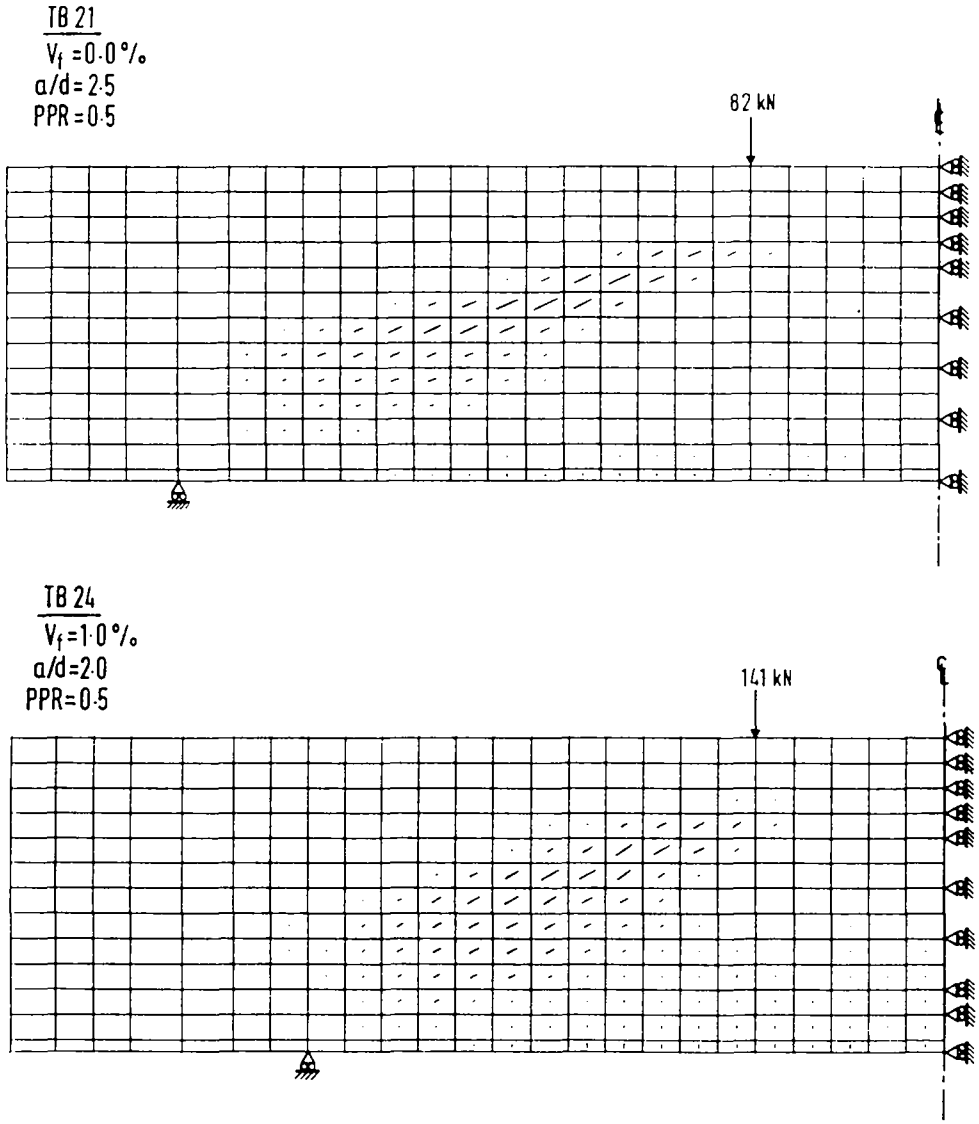

FIGURE 5. Finite element mesh and crack pattern for beams TB21 and TB24.

increment. The demec gauge readings were obtained for every 10 kN load increment. Also, the propagation of the cracks was carefully observed and marked throughout the loading process, until failure.

Results and Discussion

All beams except TB21 and TB28 failed in diagonal tension. Beam TB21 and TB28 failed in shear-compression. Typical failure patterns obtained experimentally for these beams are given in Figure 4. The failure pattern obtained from the finite element analysis for beams TB21 and TB24 along with the mesh used is given in Figure 5a and b. The crack directions (taken as the direction of the principal compressive stress) are marked through the center of each element with the length proportional to the principal tensile strain. It can be seen that the finite element formulation could predict the cracking pattern and the shear mode of failure in the beams. For beam TB21, the inclination of the cracks to the beam axis was 27° from the finite element analysis as compared to 28° in the experiment. For beam TB24, the cracks were more steeply inclined when compared to TB21, due to the reduced shear span:effective depth ratio. The inclination was 34° and 36° as determined from the finite element analysis and the experiment, respectively.

Table 2 shows the comparison of the first shear cracking load and ultimate load observed experimentally with those obtained from the finite element analysis. The predictions were closer to the experimental values for the beams with higher fiber content and tested at lower shear span:effective depth ratios. This is because the cracks are assumed to be "smeared", which is more agreeable for beams with higher fiber content or tested at lower ratios of *a:d*. It was found that the ratio of the experimental to the predicted ul-

TABLE 2. Comparison of test results with predictions

Designation	First Shear Crack Load (kN)					Ultimate Load (kN)				
	Exp	MCFT	FEM	Exp:MCFT*	Exp:FEM†	Exp	MCFT	FEM	Exp:MCFT‡	Exp:FEM§
TB21	89.6	108.2	101.2	0.83	0.89	160.2	108.8	168.0	1.47	0.95
TB22	105.4	120.4	111.4	0.87	0.95	175.0	146.0	198.0	1.20	0.88
TB23	110.0	125.4	108.6	0.88	1.01	225.9	182.4	231.0	1.24	0.98
TB24	127.2	142.2	122.8	0.89	1.04	312.7	188.0	282.0	1.62	1.11
TB25	91.0	104.2	98.2	0.87	0.93	160.0	177.0	198.0	0.91	0.81
TB26	88.2	88.8	86.8	0.99	1.02	220.1	183.2	228.0	1.20	0.97
TB27	62.2	65.6	59.2	0.95	1.11	182.3	182.2	216.0	1.00	0.85
TB28	158.0	168.2	140.0	0.94	1.12	187.0	175.6	222.0	1.06	0.84

Exp = experimental; MCFT = modified compression field theory; FEM = finite element method.
*M = 0.90, SD = 0.05.
†M = 1.01, SD = 0.08.
‡M = 1.21, SD = 0.22.
§M = 0.93, SD = 0.09.

timate load had a mean of 0.93 with a standard deviation of 0.09; the corresponding values for the shear cracking load were 1.01 and 0.08. The beam deflections, shear strains, and steel strains obtained experimentally are compared with the finite element results and the predictions based on the modified compression field theory (MCFT) [7,15] in Figures 6–9. The analytical model developed in this study utilizing the finite element method predicts the results up to the experimental ultimate load with reasonable accuracy. The MCFT approach, however, gives significantly lower ultimate loads and the reason is thought to be as follows.

The MCFT approach considered the equilibrium equations, Mohr compatibility equations, and constitutive laws for a cracked SFC element with cracks coinciding with the direction of the principal stress and strain. It involved an iterative procedure to obtain the deformation and stress distribution of a beam under a specified load. A detailed account of the procedure has been given by Tan et al. [7]. Due to the assumption of a constant shear flow across the section of the beam that was made to facilitate computation, the MCFT approach was found to predict shear failure of the beams prematurely, especially in cases where the span:effective depth ratio, a:d, is less than 2.

The influence of steel fibers on shear behavior can be seen from the results of beams TB21, TB22, and TB23 with V_f = 0.0, 0.5, and 1.0, respectively, and a PPR of 0.5. As indicated in Table 2, there is a marginal increase in first shear cracking load with an increase in the volume fraction of the fibers. However, it is seen that the ultimate loads increased by 40% with the addition of 1% of steel fibers. This is attributed to the effectiveness of the fibers in arresting the crack growth after the appearance of first shear crack as is evident from the deformation characteristics of the beams TB21 and TB23 (see Figures 6 and 7). Both the finite element

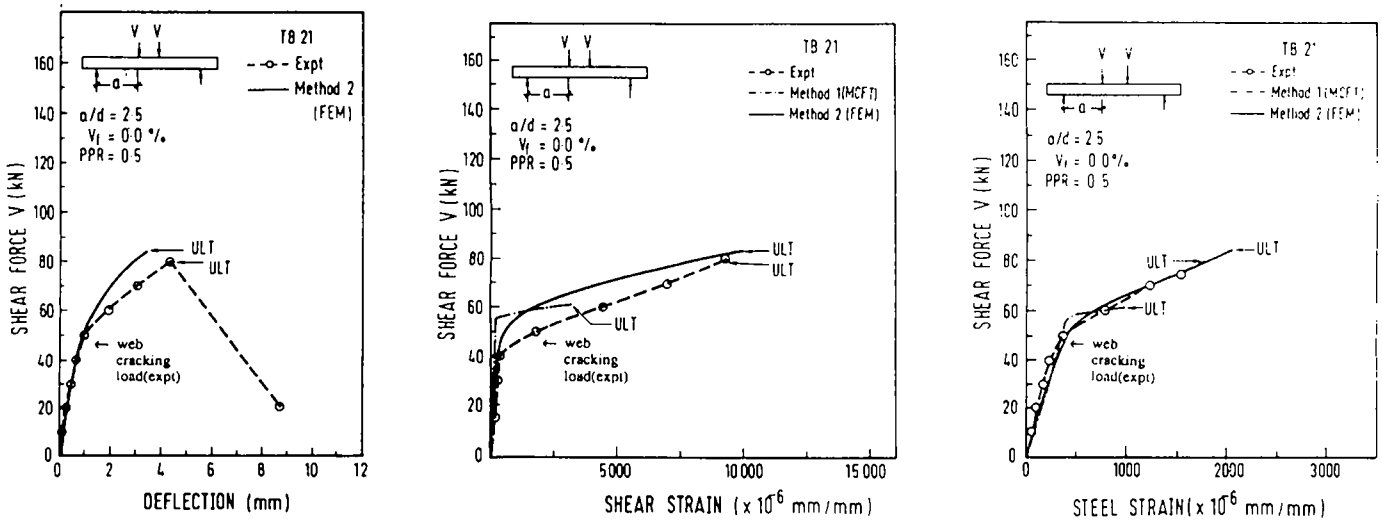

FIGURE 6. Comparison of deformations for beam TB21.

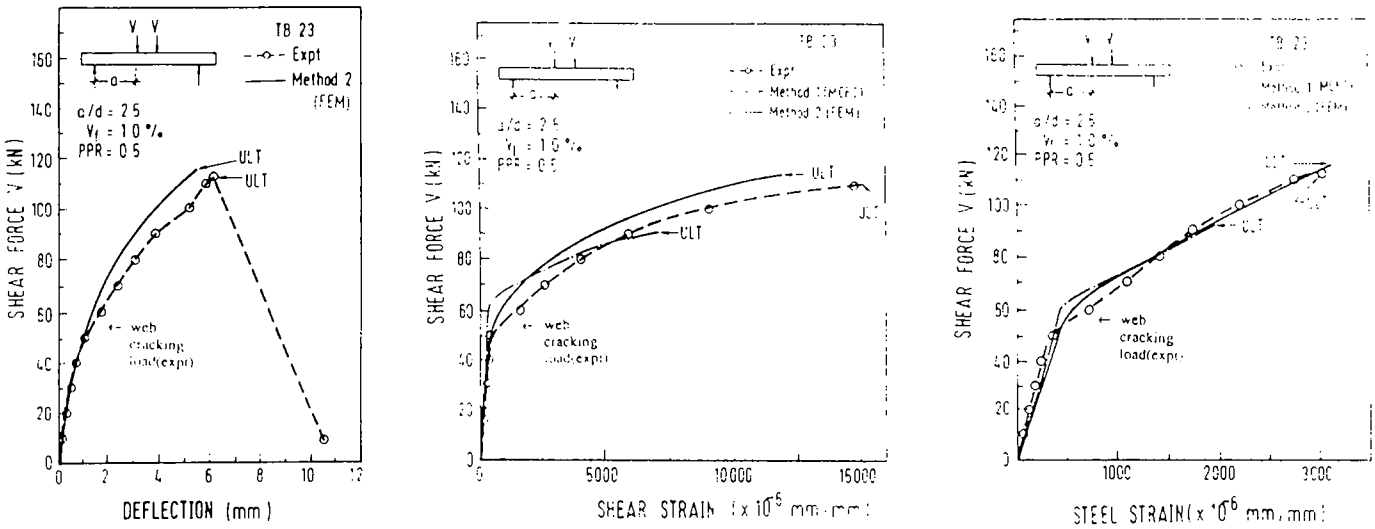

FIGURE 7. Comparison of deformations for beam TB23.

results and the experimental data indicate that the stiffness of the beam after the occurrence of the first shear crack increases with an increase in fiber content, as can be seen from the load deflection curves (Figures 6a and 7a). The same trend was observed in the shear strains (Figures 6b and 7b) and the steel strains (Figures 6c and 7c) in the shear span at a section "d" from the loading point.

Beams TB25, TB23, and TB24 each had a steel fiber content of 1.0% with a PPR of 0.5. The shear span:effective depth ratio was 3.0, 2.5, and 2.0, respectively. Table 1 shows that the smaller the shear span:effective depth ratio, the higher the first shear cracking load and the ultimate shear strength. The midpoint deflections reduced with a reduction in the shear span:depth ratio, as can be seen from Figures 7a and 8a. Also, for a given load, the shear strains (Figures 7b and 8b) and the steel strains (Figures 7c and 8c) reduced with a reduction in the shear span:effective depth ratio. It is found that the behavior of these beams was also accurately predicted by the finite element formulation.

Beams TB28, TB23, TB26, and TB27 had a steel fiber volume fraction of 1% and a PPR of 1.0, 0.5, 0.25, and 0.0, respectively, and each loaded at an *a:d* ratio of 2.5. It was observed that with an increase in the PPR, the first shear crack appeared at a higher load. The increase in this load for the partially prestressed beams when compared to the fully reinforced beam (TB27) was approximately equal to the decompression moment. The change in ultimate shear strength was approximately 20%, 22%, and −5% for an increase in PPR from 0.0 to 0.25, 0.50, and 1.0, respectively. The

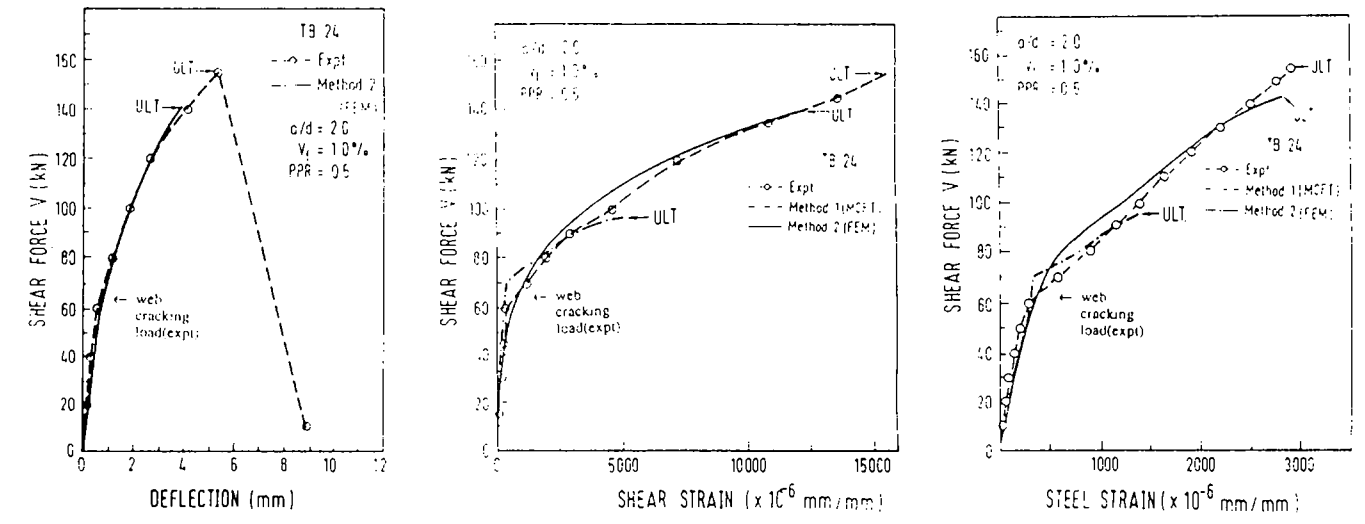

FIGURE 8. Comparison of deformations for beam TB24.

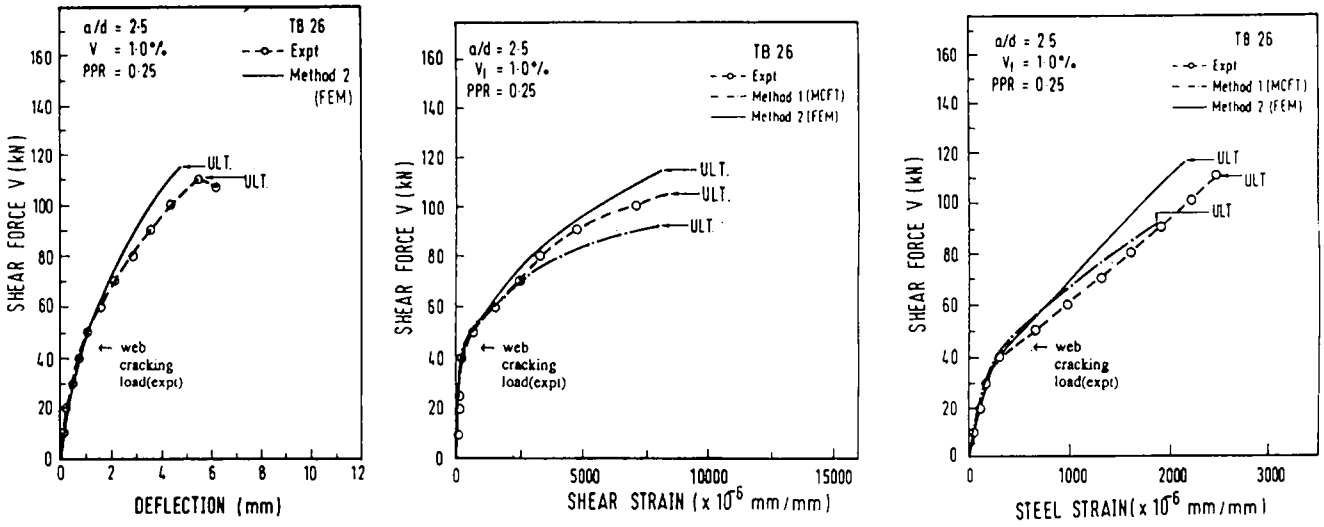

FIGURE 9. Comparison of deformations for beam TB26.

stiffness after the first shear crack was found to be lower with increasing PPR, because the total area of steel was less. This is evident from the load-deflection curves (Figures 7a and 9a), the load versus shear strain curves (Figures 7b and 9b), and the load versus steel strain curves (Figures 7c and 9c). This trend was also well predicted by the finite element formulation.

Conclusion

A finite element formulation to predict the shear behavior of partially prestressed SFC beams is presented. It is found that the finite element formulation could predict accurately the failure mode and ultimate loads for the test beams. Also, the shear strain and the steel strains obtained from the finite element analysis showed good correlation with the experimental observations. The results clearly indicate that the addition of steel fibers significantly improves the behavior of partially prestressed concrete beams, especially after the appearance of shear cracks. The presence of the steel fibers increases the stiffness of the beams after the shear cracking and results in enhanced shear strength.

Acknowledgments

The study reported in this paper forms a part of the research program supported by the National University of Singapore Research Grant RP880646.

References

1. Batson, G.; Jenkins, E.; Spatney, R. *ACI J.* **1972,** *69,* 640–644.
2. Swamy, R.N.; Bahia, H.M. *Concr. Inter. Design Construct.* **1985,** *7,* 35–40.
3. Sharma, A.K. *ACI J.* **1986,** *83,* 624–628.
4. Mansur, M.A.; Ong, K.C.G.; Paramasivam, P. *J. Struct. Eng.* **1986,** *112,* 2066–2079.
5. Lim, T.Y.; Paramasivam, P.; Lee, S.L. *Mag. Concr. Res.* **1987,** *39,* 148–160.
6. Narayanan, R.; Darwish, I.Y.S. *ACI Struct. J.* **1987,** *84,* 216–227.
7. Tan, K.H.; Murugappan, K.; Paramasivam, P. *ACI Struct. J.* **1993,** *90,* 3–11.
8. Balaguru, P.; Ezeldin, A. In *Fiber Reinforced Concrete: Properties and Applications,* ACI SP-105; Shah, S.P.; Batson, G.B., Eds.; American Concrete Institute: Detroit, MI, **1987;** pp 419–436.
9. Narayanan, R.; Darwish, I.Y.S. *Inter. J. Cem. Compos. Lightweight Concr.* **1987,** *9,* 81–90.
10. British Standard Institution. *The Structural Use of Concrete, Part 1, Design, Materials, and Workmanship,* CP110; BSI: London, **1972,** p 154.
11. Lim, T.Y.; Paramasivam, P.; Lee, S.L. *ACI Mater J.* **1987,** *84,* 286–298.
12. Murugappan, K.; Paramasivam, P.; Tan, K.H. In *Fibre Reinforced Cement and Concrete;* Swamy, R.N., Ed.; E & FN Spon: London, **1992;** pp 447–463.
13. Vecchio, F.J. *J. Struct. Eng.* **1990,** *116,* 730–750.
14. Harajli, M.H.; Naaman, A.E. *J. Struct. Eng.* **1985,** *111,* 1602–1618.
15. Tan, K.H.; Murugappan, K.; Paramasivam, P. *ACI Struct. J.* **1995** (July/August), 92.